Nanoscale

Accepted Manuscript

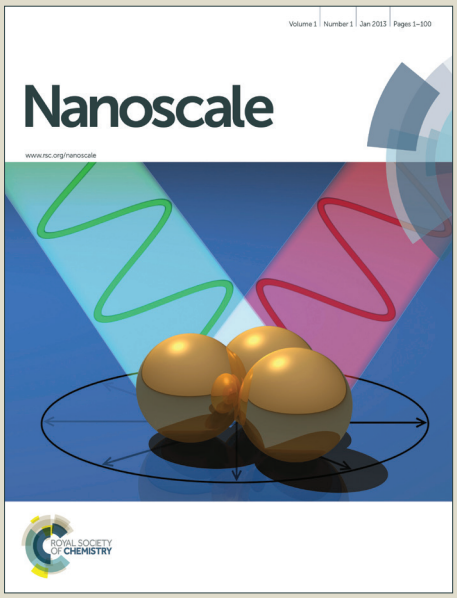

This is an *Accepted Manuscript*, which has been through the Royal Society of Chemistry peer review process and has been accepted for publication.

Accepted Manuscripts are published online shortly after acceptance, before technical editing, formatting and proof reading. Using this free service, authors can make their results available to the community, in citable form, before we publish the edited article. We will replace this *Accepted Manuscript* with the edited and formatted *Advance Article* as soon as it is available.

You can find more information about *Accepted Manuscripts* in the Information for Authors.

Please note that technical editing may introduce minor changes to the text and/or graphics, which may alter content. The journal's standard Terms & Conditions and the Ethical guidelines still apply. In no event shall the Royal Society of Chemistry be held responsible for any errors or omissions in this *Accepted Manuscript* or any consequences arising from the use of any information it contains.

ROYAL SOCIETY OF CHEMISTRY

www.rsc.org/nanoscale

In Situ Powder X-ray Diffraction Study of Magnetic $CoFe_2O_4$ Nanocrystallite Synthesis

Henrik L. Andersen and Mogens Christensen*

Center for Materials Crystallography, Department of Chemistry and iNANO, Langelandsgade 140, DK-8000 Aarhus C, Denmark.

Keywords
Spinel, ferrite, *in situ*, powder diffraction, hydrothermal, size distribution, Rietveld, whole powder pattern modelling, superparamagnetic, single-domain, nanoparticles.

Abstract
The evolution of size and size distribution during hydrothermal synthesis of nanocrystalline $CoFe_2O_4$ has been studied by *in situ* synchrotron powder X-ray diffraction (PXRD). Varying synthesis temperature or [OH^-] concentration in the precursor proves to have no significant effect on the final volume-weighted nanocrystallite sizes (~12 nm) of $CoFe_2O_4$. However, analysis by whole powder pattern modeling of the [OH^-] concentration series reveals a substantial difference in the number-weighted size distributions when varying the amount of base used. Furthermore, changing the metal ion concentration prior to NaOH addition in the precursor preparation gives a handle to control the nanoparticle sizes (~5-15 nm). All *in situ* experiments show almost instantaneous formation of the $CoFe_2O_4$ nanocrystallites, without significant growth or broadening of the size distribution after 60 s. Magnetic hysteresis curve measurements illustrate, how this facilitates the tailoring of materials with specific magnetic properties, as larger particles (~15 nm) exhibit hard magnetic properties while the smaller particles (~6-7 nm) are superparamagnetic.

Introduction
Magnetic spinel ferrite, MFe_2O_4 (M = Co^{2+}, Cu^{2+}, Ni^{2+}, etc.), are very important magnetic materials with many modern technological applications.[1] Notably, $CoFe_2O_4$ has a large magnetic anisotropy, high abundance and excellent chemical stability as well as a good saturation magnetization, mechanical hardness and relatively high Curie temperature (~793 K).[2] This makes $CoFe_2O_4$ an important magnetic material with a wide range of uses in e.g. magnetic recording media, ferrofluids and biomedicine.[3]

Controlling the size and size distribution during $CoFe_2O_4$ nanocrystallite synthesis is a key issue as the electrical, optical and magnetic properties are highly dependent on the crystallite size.[4] Larger crystallites lower their magnetostatic energy by introducing magnetic domains with different respective directions of magnetization. This division into domains reduces the coercivity of the material and also lowers the potential volume-weighted saturation magnetization due to non-contributing domain walls. On the other hand, reducing the crystallite size below the superparamagnetic limit (D_{sp}), results in zero magnetization at room temperature, due to the random spin reorientation in zero field conditions. The highest possible coercivity is achieved in the intermediate regime at the critical single-domain crystallite size (D_{sd}).

Nanoscale Accepted Manuscript

Nanosized $CoFe_2O_4$ crystallites have previously been synthesized by a broad range of methods including microemulsion techniques,[3] sol-gel autocombustion,[5] thermal decomposition,[6] solvothermal synthesis,[7] and hydrothermal synthesis.[8] The preparation of spinel ferrite nanocrystallites with specific characteristics is often a tedious process involving multiple complicated steps and size selection processes are often necessary to achieve a monodisperse product.[9] Considering the mentioned preparation pathways, the hydrothermal method has the benefit of being simple, cheap, energy efficient and easily scalable. In addition, nanocrystallite characteristics are in many cases tunable by simple adjustments to reaction parameters such as; temperature, precursor concentration, pH, pressure and reaction time.[10-12]

In this work, the size and size distribution evolution of $CoFe_2O_4$ nanocrystallites during hydrothermal synthesis is studied by *in situ* synchrotron powder X-ray diffraction (PXRD). The *in situ* characterization by the PXRD method allows the identification of optimal synthesis parameters for specific material characteristics by studying the crystal and nanostructure evolution during crystallization. By measuring *in situ*, the time needed to map parameter space is significantly reduced and the risk of post processing steps affecting the results is removed. The efficiency and advantages of the technique has been proven by several recent studies.[13-18] This is to the best of our knowledge the first investigation employing *in situ* PXRD to study the hydrothermal formation and growth of $CoFe_2O_4$ nanocrystallites.

Three series of experiments have been performed, investigating the effect of (I) synthesis temperature, (II) excess $[OH^-]$ in the precursor, and (III) metal ion concentration upon NaOH addition in the precursor preparation, on $CoFe_2O_4$ nanocrystallite sizes during hydrothermal synthesis. From the *in situ* PXRD data, crystallite sizes and size distributions are extracted by Rietveld refinement and whole powder pattern modeling (WPPM). The PXRD sizes are complemented by particle sizes found from transmission electron microscopy (TEM) images. The intrinsic volume weighting of the PXRD experiments are taken into consideration when comparing sizes and size distributions to the number-weighted TEM sizes. Finally, the magnetic hysteresis curves of selected samples have been measured to investigate the effect of $CoFe_2O_4$ nanocrystallite size on the magnetic properties.

Experimental Section

Precursor Preparation

The general experimental procedure is illustrated in Figure 1 and an overview of the investigated samples is shown in Table 1. A detailed description of the steps followed in the preparation of all the precursors can be found in the supporting information.

Precursor solutions of 2.0 M $Fe(NO_3)_3{\cdot}9H_2O$ (Sigma-Aldrich, reagent grade) and 2.0 M $Co(NO_3)_2{\cdot}6H_2O$ (Sigma-Aldrich, reagent grade) were mixed in a stoichiometric ratio of 2:1 in a syringe. An excess amount of 16.0 M NaOH (Sigma-Aldrich, reagent grade) solution was added dropwise to the mixture under magnetic stirring. Upon addition of the base, a gel formed which was suspended and homogenized by magnetic stirring and vigorous mechanical mixing. For the temperature series, an amount of NaOH corresponding to 1.25 times the molar amount of NO_3^- ions was added to the solution. For the $[OH^-]$ series, larger excesses of NaOH, i.e. 1.5 and 2.0 times the molar amount of NO_3^- ions, were added to the solution. In all cases, a final metal ion concentration of 1.2 M was obtained by subsequent addition of demineralized water.

Nanoscale Accepted Manuscript

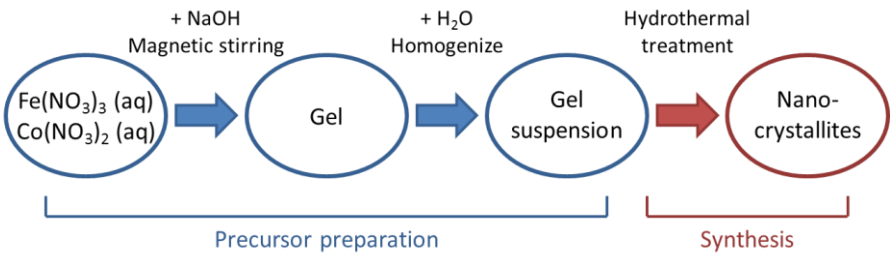

Figure 1: Schematic illustration of the general experimental procedure.

An additional series of experiments, investigating the effect of metal ion concentrations upon addition of the base during the preparation of the precursor, was performed during a second beamtime. The metal ion concentration prior to NaOH addition was varied by the addition of demineralized water to the metal-ion solutions. An amount of NaOH corresponding to 1.0 times the molar amount of NO_3^- ions in the solution was added at metal ion concentrations of 2.0 M, 1.0 M and 0.5 M respectively. In this series of experiments, a less concentrated NaOH solution of 12.0 M was used in the precursor preparation. Again, a gel formed when the base was added. For all three precursors in the series, a final metal ion concentration in the gel suspension of 0.45 M was achieved by subsequent addition of demineralized water.

Table 1: Schematic overview of the performed experiments. For convenience, CFO_270C and CFO_OH_1.25 have been assigned different names even though it is the same sample.

Sample name *(Series)*	**Synthesis temp.**	**NO_3^- : OH^-**	**Metal ion conc. Upon NaOH addition**	**NaOH conc.**	**Final metal ion conc.**
Temperature:					
CFO_170C	**170 °C**	1 : 1.25	2.0 M	16.0 M	1.2 M
CFO_270C	**270 °C**	1 : 1.25	2.0 M	16.0 M	1.2 M
CFO_320C	**320 °C**	1 : 1.25	2.0 M	16.0 M	1.2 M
CFO_370C	**370 °C**	1 : 1.25	2.0 M	16.0 M	1.2 M
[OH^-] conc.:					
CFO_OH_1.25	270 °C	**1 : 1.25**	2.0 M	16.0 M	1.2 M
CFO_OH_1.5	270 °C	**1 : 1.5**	2.0 M	16.0 M	1.2 M
CFO_OH_2.0	270 °C	**1 : 2.0**	2.0 M	16.0 M	1.2 M
Metal ion conc.:					
CFO_M_2.0	270 °C	1 : 1.0	**2.0 M**	12.0 M	0.45 M
CFO_M_1.0	270 °C	1 : 1.0	**1.0 M**	12.0 M	0.45 M
CFO_M_0.5	270 °C	1 : 1.0	**0.5 M**	12.0 M	0.45 M
Reference:					
FFO_test	270 °C	1 : 1.0	2.0 M	12.0 M	0.45 M

In order to investigate the effect of having $Co(NO_3)_2{\cdot}6H_2O$ present in the precursor, a reference experiment was performed. For this, an additional precursor without $Co(NO_3)_2{\cdot}6H_2O$ was prepared, following the same steps as above. A solution of 2.0 M $Fe(NO_3)_3{\cdot}9H_2O$ was added 12.0 M NaOH corresponding to a 1:1.0 ratio between NO_3^- and NaOH. Demineralized water was again added to get a final metal ion concentration of 0.45 M in the precursor. From here on the various experiments will be referred to by their sample name.

In Situ Powder X-ray Diffraction Measurements

The working principle of the *in situ* PXRD setup is illustrated in the supporting information and a detailed description was published by Becker et al.[19] The precursor solution/gel suspension is injected into a single crystal sapphire capillary reactor with and inner and outer diameter of 0.7 mm and 1.3

Nanoscale Accepted Manuscript

mm, respectively. The capillary is mounted using Swagelok fittings and pressurized with demineralized water using a HPLC pump. An experiment is started by simultaneously initiating the sequential X-ray exposures and switching the jet of hot air towards the sample. The small sample volume and the efficiency of the heater ensure a very rapid heating of the precursor and the desired temperature is reached within seconds causing crystallization of nanocrystallites. The monochromatic synchrotron beam diffracts from the sample and the crystallization can be monitored by measuring and analyzing the resulting PXRD patterns with the desired time resolution.

The presented *in situ* PXRD experiments were conducted during two different beamtimes at the beamline I711, MAX-II, MAX-lab, Lund, Sweden, with wavelengths around 1.0 Å and the detector positioned ~90 mm behind the sample. The wavelength, sample to detector distance and instrumental contribution to the peak broadening of the diffraction patterns in the given beamtime were determined by calibration with a NIST LaB_6 standard. The pressure was kept at 250 bar in all the experiments, while the synthesis temperature was varied between 170 and 370 °C. The actual temperature of the capillary is slightly lower than the set temperature of the heater. Heating profiles for the *in situ* PXRD setup may be found in the Supporting Information. The diffraction data was collected with an Oxford Diffraction CCD TITAN detector with a diameter of 16.5 cm. A time resolution of 5 s was attained using an exposure time of 4 s and a detector readout time of 1 s.

Rietveld Refinement

The raw data frames were integrated in *Fit2D,*[20] and subsequently analysed by sequential Rietveld refinement using *FullProf Suite.*[21] The refinements of the cobalt ferrites were done based on the structure of $CoFe_2O_4$ in the cubic *Fd*-3*m* space group illustrated in Figure 2. In theory, $CoFe_2O_4$ favours the inverse spinel, $[Fe^{3+}]^{tet}[Co^{2+},Fe^{3+}]^{oct}O_4$, structure.[22] However, the actual cation distribution between octahedral and tetrahedral sites in the $CoFe_2O_4$ is known to deviate.[23-25] Distinguishing between Fe and Co with PXRD is not straightforward due to the similar scattering powers of the two neighboring elements. Here, the spinel inversion ratio is thus assumed random. Detailed information about the refinements may be found in the supporting information.

Nanoscale Accepted Manuscript

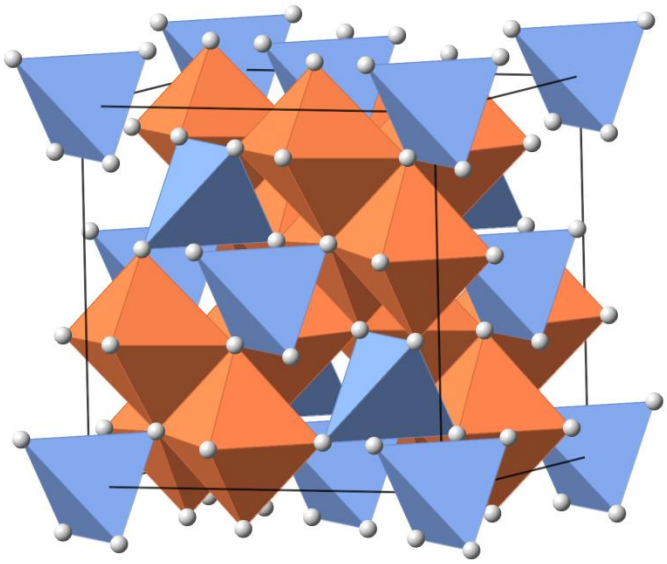

Figure 2: Illustration of the cubic spinel structure of $CoFe_2O_4$. The white spheres represent the oxygen atoms, while the tetrahedral and octahedral sites are indicated with blue and orange polyhedrons respectively.

The instrumental contribution to the total peak broadening was determined using data obtained from a NIST LaB_6 standard and corrected for in the refinements. The remaining sample broadening arises from small crystallite domain sizes and microstrain in the sample. For very small crystallites the sample broadening is dominant and the microstrain contribution becomes negligible. In this work the crystallites are assumed spherical and strain free, and the sample broadening can thus be described by the Scherrer formula, $FWHM=(K\cdot\lambda)/(\langle D\rangle\cdot\cos(\theta))$,[26] from which the crystallite sizes can be determined. Here $\langle D\rangle$ is the average volume-weighted size of the coherently scattering crystalline domains, λ is the X-ray wavelength, K is the shape factor, θ is the Bragg angle and $FWHM$ describes the peak broadening (i.e., full width at half the maximum intensity of the peak).

Whole Powder Pattern Modelling

Whole powder pattern modelling (WPPM) was performed on selected diffraction patterns using the *PM2K* software.[27] The instrumental profile was determined and corrected for by fitting the Caglioti function to a NIST LaB_6 standard.[28] The background was described using a fifth degree Chebychev polynomial. Strain contributions to the peak profile were neglected and the size broadening was implemented as originating from a lognormal distribution of nanoscale scattering domains, $g(D)=(1/[D\sigma(2\pi)^{1/2}])\exp[-(1/2)([\ln D-\mu]/\sigma)^2]$.[29] Here, g is the frequency, D is the crystallite size, σ is the lognormal scale parameter and μ is the lognormal location parameter. Average volume-weighted crystallite sizes (comparable to sizes obtained from Scherrer analysis) were extracted from the resulting number-weighted size distributions by the volume-averaged formula, $\langle D\rangle=(3/4)\exp[\mu+(7/2)\sigma^2]$.[29, 30]

Transmission Electron Microscopy Measurements

Following the measurement of the sequential X-ray PXRD data, the product was carefully collected from the capillary and saved for further characterization. For specific experiments a few drops of the collected product was suspended in approximately 5 ml ethanol, sonicated for 1 h and subsequently

Nanoscale Accepted Manuscript

evaporated onto TEM-grids at room temperature. The TEM measurements were performed on a Philips CM20 running a LaB_6 cathode at 200 kV.

Magnetic Measurements

The remaining product from the TEM sample preparation was thoroughly washed with water and ethanol and subsequently dried. The small amounts of sample, i.e. $m_{CFO_M_2.0}$=1.108 mg, $m_{CFO_M_1.0}$=0.454 mg and $m_{CFO_M_0.5}$=1.794 mg, were dispersed in graphite powder (ChemPUR, >99%) and compacted into 2.5 mm diameter pellets to prevent physical movement of the particles during the experiments. A Quantum Design Physical Property Measurement System (PPMS) equipped with a Vibrating Sample Magnetometer (VSM) was used for the magnetic characterization of the nanocrystallites. The field dependent magnetization was measured by cycling the external field between +20 and -20 kOe at 300 K. The resulting hysteresis curves were corrected for the diamagnetic contribution from the graphite, which was determined by measurement of a pure graphite pellet under equivalent conditions. Additional information may be found in the supporting information.

Results and Discussion

Phase Investigation

The diffraction pattern produced by $CoFe_2O_4$ is very similar to those of Fe_3O_4 or γ-Fe_2O_3 and good refinements can be obtained using any of the three phases in the modeling. The unit cell can be used as a phase indicator due to slight differences in the lattice parameters, i.e. a(γ-Fe_2O_3) ≈ 8.33 Å < a($CoFe_2O_4$) ≈ 8.395 Å < a(Fe_3O_4) ≈ 8.396 Å at ambient conditions.[31] However, due to the broad peaks, lack of internal standard and the elevated temperature accurate determination of the lattice parameter is difficult and care must be taken not to draw any misleading conclusions. As an independent check an additional experiment was thus performed, in order to ascertain that the crystallites produced, when heating the precursors containing $Fe(NO_3)_3{\cdot}9H_2O$ and $Co(NO_3)_2{\cdot}6H_2O$, are actually $CoFe_2O_4$ nanocrystallites. The *in situ* PXRD data sets obtained during hydrothermal treatment at 250 bar and 270 °C of FFO_test and CFO_M_2.0 are shown in Figure 3 (A) and (B) respectively.

Nanoscale Accepted Manuscript

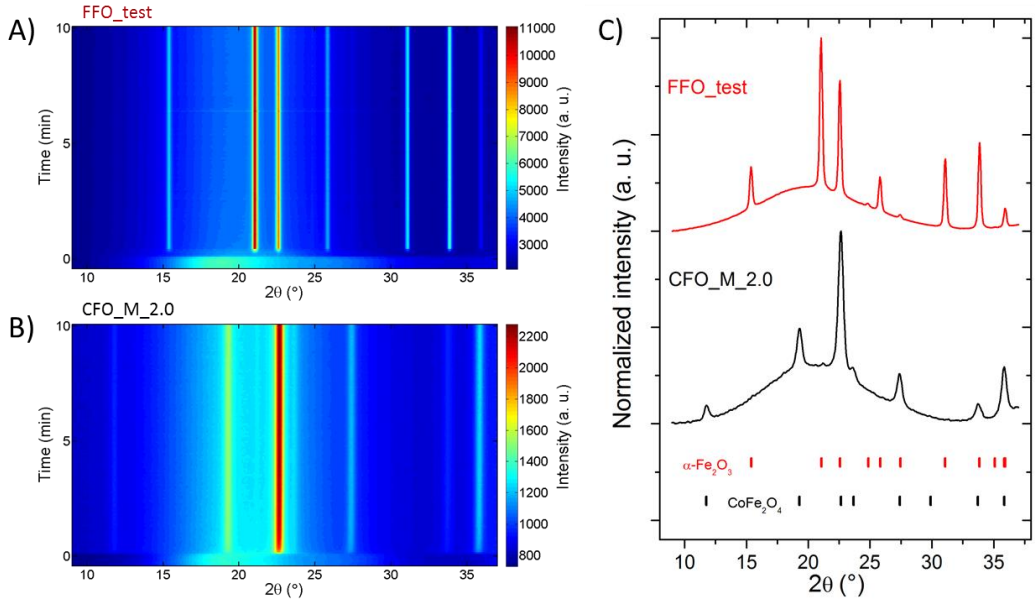

Figure 3: (A) Time resolved *in situ* PXRD data obtained during hydrothermal treatment of FFO_test at 270 °C. (B) Time resolved *in situ* PXRD data obtained during hydrothermal treatment of CFO_M_2.0 at 270 °C. (C) Comparison of *in situ* PXRD data frames obtained after 10 minutes of hydrothermal treatment of FFO_test (Red) and CFO_M_2.0 (Black) at 270 °C. The red and black marks indicate the Bragg positions of α-Fe_2O_3 in space group *R*-3*c* and $CoFe_2O_4$ in space group *Fd*-3*m* respectively.

In both experiments, the precursors crystallize almost instantly when the heat is switched towards the sample at *t*=0 min. However, two very different diffraction patterns appear. Figure 3 (C) illustrates the diffraction patterns of the two samples collected after 10 minutes of hydrothermal treatment under identical conditions. The resulting diffraction pattern of FFO_test is characterized by two intense distinctive Bragg peaks and originates from the structure of α-Fe_2O_3 in the *R*-3*c* space group. The diffraction pattern from CFO_M_2.0 clearly illustrates the effect of Co^{2+}, as the characteristic *Fd*-3*m* cubic spinel Bragg peaks are easily seen, which indicates that the product is $CoFe_2O_4$. A very weak peak at 2θ = 21.2° indicating an insignificant amount of α-Fe_2O_3 is observed in the data.

Variation of Synthesis Temperature and [OH⁻] Concentration

In the first series of experiments the effect of reaction temperature was investigated. Figure 4 (A) shows the obtained Scherrer crystallite diameters as a function of time for the same precursor treated at different temperatures, i.e. 170 °C, 270 °C, 320 °C and 370 °C. In all cases, the equilibrium crystallite size is attained within the first minute of the experiment and continued heating causes no further apparent growth of the crystallites. After 5 minutes of hydrothermal treatment of CFO_270C, CFO_320C and CFO_370C the nanocrystallites attained very similar sizes of 11.4(1) nm, 12.0(1) nm and 11.5(1) nm respectively. However, for CFO_170C slightly smaller crystallites of 9.9(1) nm was obtained, hinting the need to explore even lower reaction temperatures. Yet, the difference in $CoFe_2O_4$ nanocrystallite sizes in the explored temperature interval is not substantial enough to conclude any significant size dependence on reaction temperature.

Nanoscale Accepted Manuscript

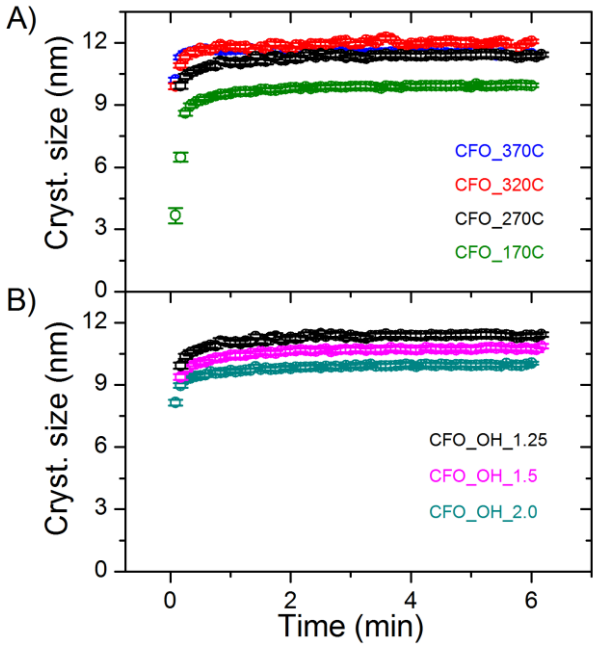

Figure 4: (A) Crystallite diameters as function of reaction time for the experiments in the temperature series. (B) Crystallite diameters as function of reaction time for the experiments in the OH^- series.

In a second series of experiments the effect of [OH^-] concentration on nanocrystallite sizes was investigated. Precursors with various excess amounts of NaOH, i.e. 1.25, 1.5 and 2.0 times the molar amount of [NO_3^-] ions were treated at 270 °C. Figure 4 (B) shows the crystallite size evolution of CFO_OH_1.25, CFO_OH_1.5 and CFO_OH_2.0. Again, equilibrium sizes were achieved almost instantly without any apparent subsequent crystallite growth. After 5 minutes of hydrothermal treatment CFO_OH_1.25 gives nanocrystallites of 11.4(1) nm, while CFO_OH_1.5 yields 10.7(1) nm crystallites and CFO_OH_2.0 gives 9.9(1) nm nanocrystallites. The observed data reveals a trend of decreasing size with increasing [OH^-] concentration. However, the difference in sizes is small and the error on an absolute scale may be underestimated using the Scherrer equation.

Evolution of Crystallite Size Distribution

The evolution of crystallite size distributions with time was investigated by WPPM analysis of selected data frames. Figure 5 (A) shows size distributions of CFO_270C after different reaction times. The WPPM analysis reveals a broadening and a shift to a larger size of the number-weighted distribution, which happen within the first 60 s of the experiment. The continued heating of the sample has no significant effect, neither on the average size nor the size distribution. In order to obtain a narrower size distribution the reaction should thus be completed and quenched within the first 20 s of the reaction.

Nanoscale Accepted Manuscript

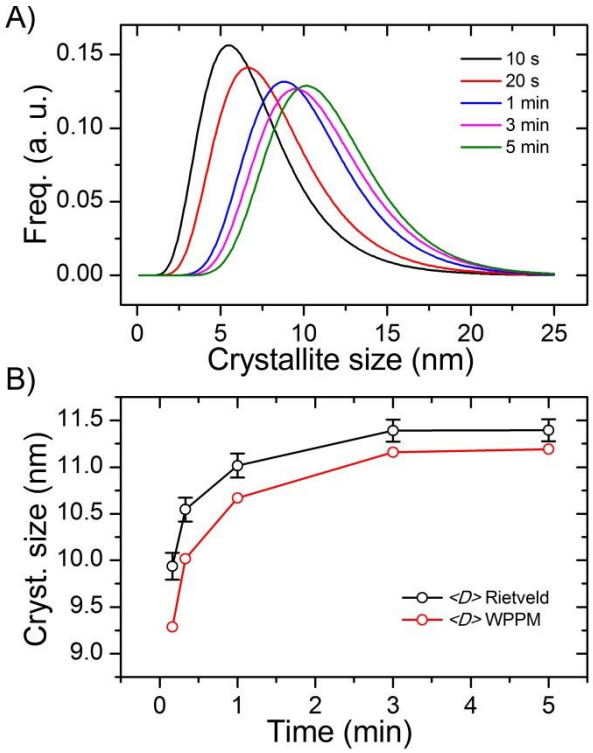

Figure 5: (A) Evolution of number-weighted lognormal size distribution for CFO_270C. (B) Comparison of volume-weighted crystallite sizes obtained at various reaction times from WPPM and Rietveld refinement of the same *in situ* PXRD data from CFO_270C. The standard deviations of the WPPM sizes are around 4 nm on an absolute scale.

Figure 5 (B) shows a comparison of the volume-weighted mean sizes obtained from Rietveld based Scherrer analysis and WPPM. The trends of the volume averaged crystallite size as function of time for the two different modeling techniques are very similar, with a small offset in the absolute sizes. The excellent agreement between the two analysis techniques affirms robustness of the size analysis.

Controlling the Size Distribution

The effect of [OH^-] concentration on the crystallite size distribution was also investigated. Crystallite size distributions from WPPM analysis of CFO_OH_1.25, CFO_OH_1.5 and CFO_OH_2.0 treated for 5 minutes at 270 °C are shown in Figure 6.

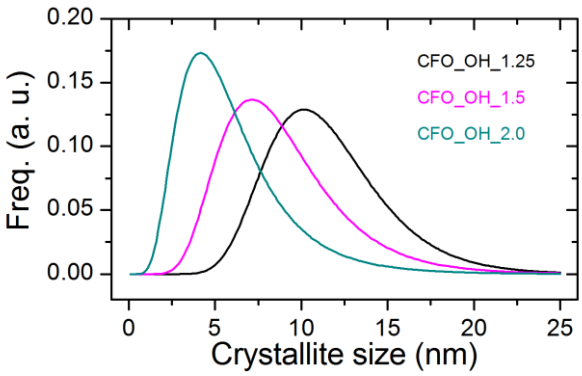

Figure 6: Number-weighted crystallite size distributions obtained by WPPM analysis of diffraction patterns obtained after 5 minutes of hydrothermal treatment at 270 °C of the indicated samples.

Nanoscale Accepted Manuscript

Modification of the precursor [OH-] concentration results in smooth variation of the obtained size distribution. The WPPM analysis reveals that varying the amount of NaOH in the precursor has a bigger impact on the crystallite size distribution than what would be expected from the very similar sizes determined in the Scherrer analysis. The difference in average volume-weighted sizes from Scherrer analysis of CFO_OH_1.25 and CFO_OH_1.5 is 1.5 nm, while the difference in the modes (global maxima) of the number-weighted distributions is ~6 nm. These results demonstrate the importance of characterizing the distribution of sizes and not just the average size of a sample.

Evolution of Crystallographic Unit Cell

No internal standard was used during the measurements of the *in situ* data and care must thus be taken when comparing absolute unit cell lengths from the different experiments. Consequently, conclusions made here are based on relative changes and general trends rather than absolute values. Figure 7 (A) and (C) show the evolution of the crystallographic unit cell with reaction time in the temperature and [OH-] concentration series, respectively. In all cases, the unit cell length *a* decreases within the first 30 seconds of the experiments after which it stabilizes at an equilibrium value.

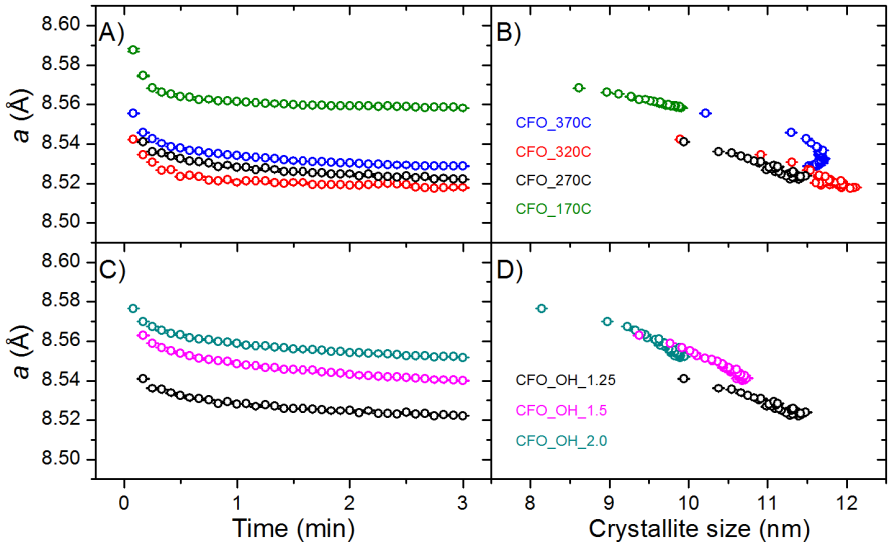

Figure 7: (A) Unit cell length *a* as a function of time in the temperature series. (B) Unit cell length *a* as a function of crystallite size in the temperature series. (C) Unit cell length *a* as a function of time in the [OH-] concentration series. (D) Unit cell length *a* as a function of crystallite size in the [OH-] concentration series.

The unit cell length *a* as a function of crystallite size for the temperature and [OH-] concentration series has been plotted in Figure 7 (B) and (D). The trend of relaxing unit cell size has been observed in several other simple oxide systems and is often attributed to reduced defect concentrations or surface relaxations associated with the increase in crystallite size.[16, 32, 33] For the investigated system, a seemingly linear decrease of *a* with crystallite size is observed. The trend is likely related to the surface to bulk ratio which decreases with 1/(crystallite radius), however a wider size range would be necessary to verify this point.

Variation of Metal Ion Concentration upon NaOH Addition

In the third series of experiments, the effect of metal ion concentration in the precursor prior to NaOH addition was investigated. Precursors with different metal ion concentrations upon NaOH addition of 2.0 M, 1.0 M and 0.5 M, but with same final metal ion concentrations, were treated hydrothermally at

Nanoscale Accepted Manuscript

270 °C. Figure 8 shows diffraction patterns obtained after 10 minutes of heating of the three different precursors. A clear difference between the peak profiles is observed. CFO_M_1.0 and CFO_M_0.5 produce similar diffraction patterns while the peaks for CFO_M_2.0 are sharper, indicating a larger size of the crystallites. A low final metal ion concentration of 0.45 M was used to allow variation the metal ion concentration upon NaOH addition, resulting in a reduced signal to noise ratio. In addition, the combination of size broadening and low intensity makes it hard to completely distinguish the diffraction peaks from the background. Consequently, the *in situ* PXRD data quality makes it challenging to reliably extract size parameters for the very small nanocrystallite sizes. In order to obtain a better estimate of the size trend, the samples have been investigated by transmission electron microscopy.

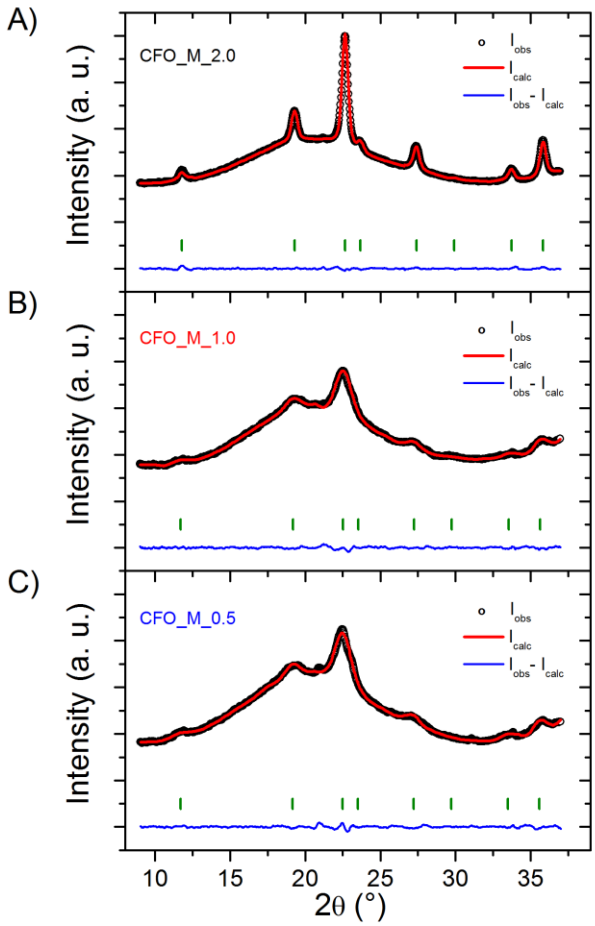

Figure 8: Powder diffraction patterns of (A) CFO_M_2.0, (B) CFO_M_1.0 and (C) CFO_M_0.5 obtained after 10 minutes of hydrothermal treatment at 250 bar and 270 °C. The data (black points) has been modeled by the Rietveld method (red line), with the blue line illustrating the difference between the measured data and the fitted model. The green ticks show the Bragg positions of $CoFe_2O_4$ in space group *Fd*-3*m*.

In all three experiments full crystallization is achieved within seconds of switching the heat toward the sample as illustrated by the normalized scale factors in Figure 9 (A). The evolution of crystallite diameters as a function of size is shown in Figure 9 (B). Again, the equilibrium size is quickly attained and no significant subsequent growth of the crystallites is observed. However, there is a considerable difference in the resulting sizes from the three precursors. CFO_M_2.0, which was prepared in the same way as the precursors in the two first series of experiments, yields crystallites of ~15 nm after

Nanoscale Accepted Manuscript

being treated at 270 °C for 10 minutes. This is slightly larger than the crystallite sizes of ~12 nm seen in the first two series of experiments. This may be an effect of the less concentrated NaOH solution (12.0 M instead of 16.0 M). CFO_M_1.0 and CFO_M_0.5 yield much smaller crystallites of ~5 nm after 10 minutes at 270 °C. The order in which NaOH and H_2O is added to the precursor is therefore of critical importance and gives a handle to control the nanocrystallite size.

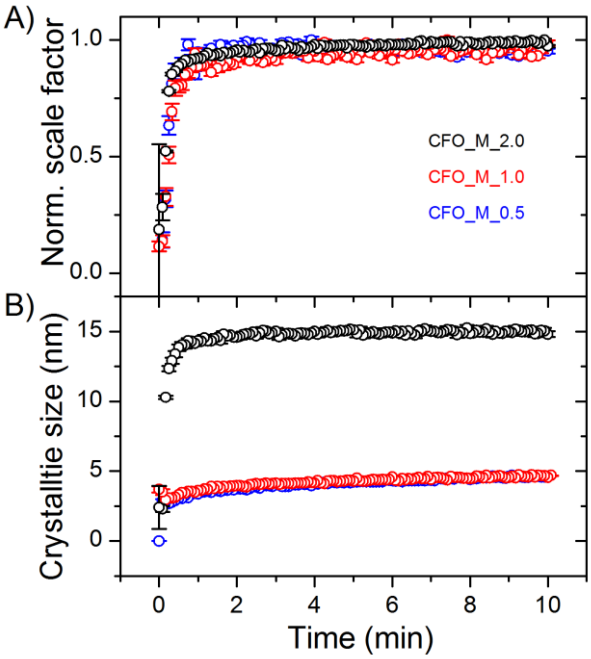

Figure 9: (A) Normalized scale factor as a function of synthesis time for the given samples at a set temperature of 270 °C. (B) Crystallite diameters as a function of time of the given samples at a set temperature of 270 °C.

Figure 10 shows the nanocrystallite size distributions obtained by WPPM analysis of CFO_M_2.0, CFO_M_1.0 and CFO_M_0.5 after 10 min of hydrothermal treatment. The distributions indicate a broadening and an increase in crystallite size with increasing metal ion concentration upon base addition. The results differ from the Scherrer sizes obtained from Rieveld analysis, where CFO_M_1.0 and CFO_M_0.5 gave identical crystallite sizes. However, this dissimilarity may be attributed to the different weightings of the analysis methods. The volume-weighted size distributions shown in the insert in Figure 10 illustrates the similarity of the volume-weighted sample sizes.

Nanoscale Accepted Manuscript

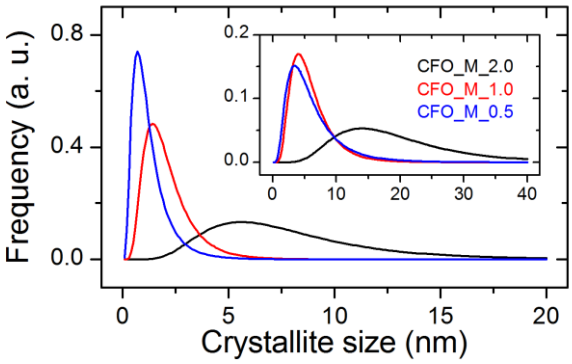

Figure 10: Number-weighted crystallite size distributions extracted from *in situ* PXRD data frames obtained after 10 minutes of hydrothermal treatment of CFO_M_2.0, CFO_M_1.0 and CFO_M_0.5. The insert shows the corresponding volume-weighted crystallite size distributions.

The factor deciding the crystallite size is most probably the structure of the gel which forms upon addition of the base. In CFO_M_2.0, the metal ion concentration was 2.0 M when the base was added, which results in a gel with a dense distribution of metal ions. The results imply that the subsequent addition of water simply suspends the gel instead of diluting the local metal ion concentration. When heat is applied, the high local concentration of metal ions thus results in relatively large crystallites being formed as the material is readily available. For CFO_M_1.0 and CFO_M_0.5, a much less concentrated gel is formed due to the dilution of the solution prior to NaOH addition, and considerably smaller crystallites are therefore obtained. However, the underlying mechanism may not be that straightforward as CFO_M_1.0 and CFO_M_0.5 give rise to almost identical crystallite sizes. In order to shed more light onto the processes governing the formation and growth of the $CoFe_2O_4$ nanocrystallites, additional studies employing total scattering and PDF (Pair Distribution Function) analysis could be conducted.[15, 34-37] Here, the atomic structure of even amorphous particles can be elucidated. Small angle scattering experiments could also be extremely useful, as this can provide information on sizes of amorphous clusters.

Particle Size and Morphology

Transmission electron microscopy images were obtained in order to verify the observed crystallite size dependency on metal ion concentration upon NaOH addition. Notably, TEM analysis provides number-weighted sizes while PXRD yields volume-weighted sizes due to the intrinsic volume-weighting of the diffraction experiment. Number-weighted sizes are generally expected to be smaller than volume-weighted sizes.[38] However, electron microscopy gives the size of the entire particle which may consist of multiple crystallites, amorphous layers, etc., while PXRD gives the averages size of coherently scattering single-crystalline domains. Comparison of absolute size from the two methods is not straightforward but the images provide useful information on particle morphology and size trends. Figure 11 shows TEM images and corresponding size analyses of product from CFO_M_2.0, CFO_M_1.0 and CFO_M_0.5, which has been carefully washed out of the capillary subsequent to *in situ* PXRD characterization.

Nanoscale Accepted Manuscript

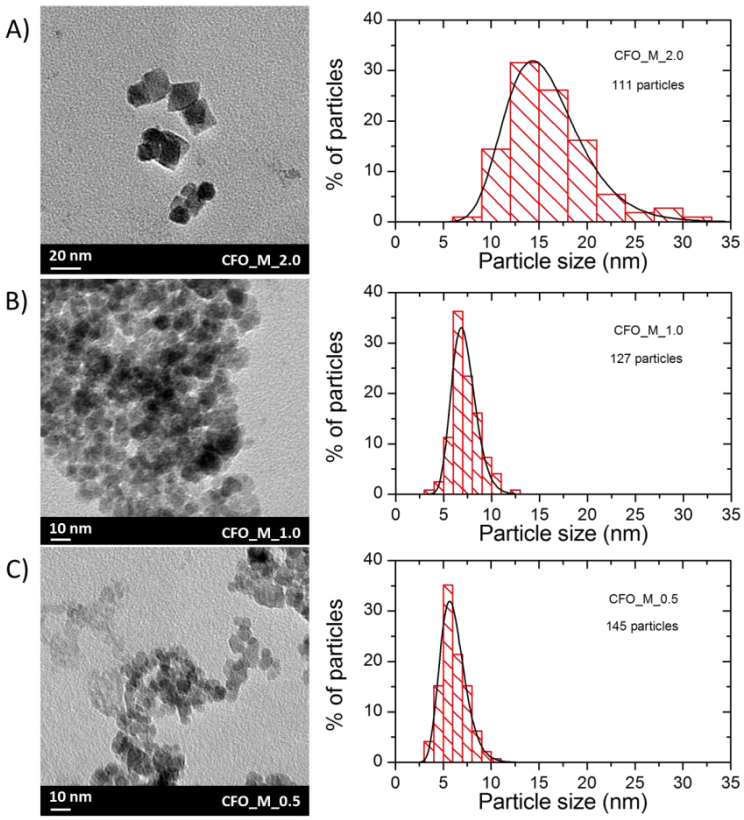

Figure 11: TEM micrographs of product collected after hydrothermal treatment of CFO_M_2.0 (A), CFO_M_1.0 (B) and CFO_M_0.5 (C) at 270°C and 250 bar. Size analyses are shown next to their corresponding representative TEM pictures. The histograms have been fitted by a lognormal distribution from which the average particle size has been extracted.

The TEM micrographs and the size analysis confirm the size trends observed by Scherrer analysis and WPPM. The size analyses are based on manual measurements of the indicated number of particle sizes from different TEM micrographs of the same sample. The resulting histograms have been fitted by lognormal distributions from which the average particle size is extracted. CFO_M_2.0 again yields much larger particles of 15.8(1) nm, while CFO_M_1.0 and CFO_M_0.5 give particles of 7.2(1) and 6.1(1) nm respectively. However, the absolute particles sizes are slightly larger than the PXRD sizes. Interestingly, the smaller particles seem to have spherical morphology while particles above ~20 nm tend to have cubic or octahedral shape. Shape control of $CoFe_2O_4$ nanoparticles has previously been reported.[39] In the following section the number-averaged TEM sizes will be used to describe the size of the prepared particles and to distinguish the samples.

Magnetic Hysteresis

The field dependent magnetization curves measured at room temperature are shown in Figure 12. The largest particles of 15.8 nm exhibit hard magnetic properties with a coercivity of 1568(8) Oe. The smaller particles of 7.2 and 6.1 nm have very low coercivities of 45(2) and 4(4) Oe respectively. The trend indicates that the particles are all below the critical single-domain particle size D_{sd}, which is in good agreement with a previously experimentally estimated D_{sd} of ~40 nm.[40]

Nanoscale Accepted Manuscript

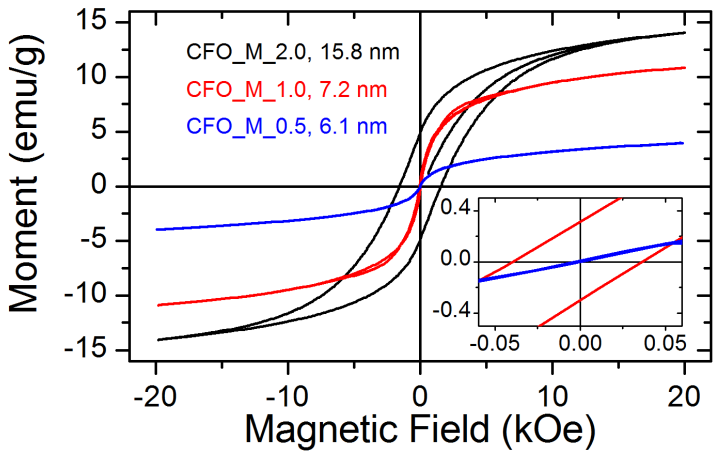

Figure 12: Magnetic moment versus applied magnetic field of the indicated samples measured at 300 K. The insert shows an enhancement of the small applied field region. The hysteresis curve has not been corrected for the samples self-demagnetization.

A size dependency of the magnetic remanence and saturation magnetization is also observed. The 15.8 nm sample attains a magnetization of 14.1(1) emu/g in an applied field of +20 kOe and a magnetic moment of 4.87(1) emu/g is retained when the external field is subsequently reduced to zero. The 7.2 nm sample has a saturation magnetization of 10.9(3) emu/g and a remanence of 0.32(1) emu/g while the 6.1 nm sample saturates at 3.98(2) emu/g and retains a remanence of 0.01(1) emu/g. The trend with larger particles attaining higher magnetization is observed for several magnetic ferrites[4, 41] and other metal-oxide systems.[42]

The reduction of coercivity and magnetization may be attributed to the particle sizes being in the superparamagnetic regime. This is confirmed by the typical S-shape of the curve with near zero coercivity.[43] For superparamagnetic particles the time between magnetization reversals τ is given by the Néel-Brown law, $\tau=\tau_0\exp(K_1V/k_BT)$, where τ_0 is the attempt time (~1 ns), K_1 is the effective anisotropy constant, k_B is the Boltzmann constant and T is the temperature.[2] By setting the flipping time equal to the measurement time τ_M the critical superparamagnetic threshold diameter D_{sp} can be estimated by, $D_{sp}=[-6k_BT\ln[\tau_M/\tau_0]/(\pi K_1)]^{1/3}$. Based on bulk material parameters (K_1=0.270 MJ/m^3) a D_{sp} of 8.4 nm for spherical $CoFe_2O_4$ nanoparticles at room temperature can be calculated.[2] This agrees very well with the observed results as only the CFO_M_2.0 sample, which has a particle diameter above this threshold, exhibits significant hysteresis.

Conclusions

In situ studies of the hydrothermal synthesis of $CoFe_2O_4$ show no significant crystallite size dependence on synthesis temperature or precursor [OH$^-$] concentration. However, having different concentrations of metal ions in the solution, when adding the NaOH during precursor preparation, proves to have a huge influence on the size of the nanocrystallites. A metal ion concentration of 2.0 M yields 15.8(1) nm particles while concentrations of 1.0 and 0.5 M gives 7.2(1) and 6.1(1) nm particles respectively. An amorphous particle formation most probably takes place when adding the NaOH to the precursor solution, with the heating facilitating crystallization. Analysis by whole powder pattern modeling of the [OH$^-$] concentration series reveals a substantial difference in number weighted size distributions when varying the amount of base used. Magnetic hysteresis measurements of the synthesized particles show a size dependence of the magnetic properties. The reported synthesis

Nanoscale Accepted Manuscript

methods thus give a handle to control not only the particles sizes, size distributions, and crystal shape, but also the magnetic properties of the final $CoFe_2O_4$ nanoparticle product.

Associated Content

Considerations on the effect of crystallite size on the magnetic properties. Details regarding the precursor preparations. Temperature profiles for the *in situ* PXRD setup. Detailed descriptions of the data integration and sequential Rietveld refinement procedures. Considerations regarding TEM particle sizes. Detailed description of magnetic data treatment.

Author Information

Corresponding Author

*E-mail: mch@chem.au.dk

Notes

The authors declare no competing financial interest.

Acknowledgements

This work was supported by the Danish Research Council for Technology and Production Sciences (Improved Permanent Magnets through Nanostructuring), the Danish Research Council for Nature and Universe (DanScatt), the Danish National Research Foundation (Center for Materials Crystallography, DNRF93) and partially funded by the European Community through the Seventh Framework Programme under grant agreement no. 310516 (Nanopyme). The authors are grateful for the obtained beamtimes at beamline I711, MAX-lab synchrotron radiation source, Lund University, Sweden. Carsten Gundlach, Dörthe Haase, Diana Thomas and Francisco Martinez are thanked for their support during the beamtimes. Kirsten M. Ø. Jensen and Espen D. Bøjesen are thanked for their help with experiments and data analysis.

References

1. R. Valenzuela, *Physics Research International*, 2012, **2012**.
2. R. Skomski, *J. Phys.: Condens. Matter*, 2003, **15**, R841-R896.
3. D. S. Mathew and R. S. Juang, *Chem. Eng. J.*, 2007, **129**, 51-65.
4. M. Artus, L. B. Tahar, F. Herbst, L. Smiri, F. Villain, N. Yaacoub, J.-M. Grenèche, S. Ammar and F. Fiévet, *J. Phys.: Condens. Matter*, 2011, **23**, 506001.
5. L. H. Ai and J. Jiang, *Curr. Appl Phys.*, 2010, **10**, 284-288.
6. T. Hyeon, Y. Chung, J. Park, S. S. Lee, Y. W. Kim and B. H. Park, *J. Phys. Chem. B*, 2002, **106**, 6831-6833.
7. S. H. Sun, H. Zeng, D. B. Robinson, S. Raoux, P. M. Rice, S. X. Wang and G. X. Li, *J. Am. Chem. Soc.*, 2004, **126**, 273-279.
8. W. J. Schuele and V. D. Deetscreek, *J. Appl. Phys.*, 1961, **32**, S235-S236.
9. T. Hyeon, *Chem. Commun.*, 2003, 927-934.
10. C. Aymonier, A. Loppinet-Serani, H. Reveron, Y. Garrabos and F. Cansell, *J. Supercrit. Fluids*, 2006, **38**, 242-251.
11. R. I. Walton, *Chem. Soc. Rev.*, 2002, **31**, 230-238.
12. M. Yoshimura and K. Byrappa, *J. Mater. Sci.*, 2008, **43**, 2085-2103.
13. K. M. Ø. Jensen, C. Tyrsted, M. Bremholm and B. B. Iversen, *ChemSusChem*, 2014, **7**, 1594–1611.
14. C. Tyrsted, K. M. Ø. Jensen, E. D. Bojesen, N. Lock, M. Christensen, S. J. L. Billinge and B. B. Iversen, *Angew. Chem. Int. Ed.*, 2012, **51**, 9030-9033.
15. K. M. Ø. Jensen, M. Christensen, P. Juhas, C. Tyrsted, E. D. Bojesen, N. Lock, S. J. L. Billinge and B. B. Iversen, *J. Am. Chem. Soc.*, 2012, **134**, 6785-6792.

Nanoscale Accepted Manuscript

16. H. L. Andersen, K. M. Ø. Jensen, C. Tyrsted, E. D. Bøjesen and M. Christensen, *Cryst. Growth Des.*, 2014, **14**, 1307-1313.
17. P. Nørby, S. Johnsen and B. B. Iversen, *ACS Nano*, 2014, **8**, 4295-4303.
18. E. D. Bøjesen, K. M. Ø. Jensen, C. Tyrsted, N. Lock, M. Christensen and B. B. Iversen, *Cryst. Growth Des.*, 2014, **14**, 2803-2810.
19. J. Becker, M. Bremholm, C. Tyrsted, B. Pauw, K. M. Ø. Jensen, J. Eltzholt, M. Christensen and B. B. Iversen, *J. Appl. Crystallogr.*, 2010, **43**, 729-736.
20. A. P. Hammersley, S. O. Svensson, M. Hanfland, A. N. Fitch and D. Hausermann, *High Pressure Research*, 1996, **14**, 235-248.
21. J. Rodriguez-Carvajal, *Physica B*, 1993, **192**, 55-69.
22. Y. H. Hou, Y. J. Zhao, Z. W. Liu, H. Y. Yu, X. C. Zhong, W. Q. Qiu, D. C. Zeng and L. S. Wen, *J. Phys. D: Appl. Phys.*, 2010, **43**, 445003.
23. G. A. Sawatzky, F. Van der Woude and A. H. Morrish, *J. Appl. Phys.*, 1968, **39**, 1204-1205.
24. M. R. Deguire, R. C. Ohandley and G. Kalonji, *J. Appl. Phys.*, 1989, **65**, 3167-3172.
25. Y. M. Abbas, S. A. Mansour, M. H. Ibrahim and S. E. Ali, *J. Magn. Magn. Mater.*, 2011, **323**, 2748-2756.
26. B. E. Warren, *X-ray Diffraction*, Dover Publications, Mineola, 1990.
27. M. Leoni, R. Maggio, S. Polizzi and P. Scardi, *J. Am. Ceram. Soc.*, 2004, **87**, 1133–1140.
28. G. Caglioti, A. Paoletti and F. P. Ricci, *Nuclear Instruments*, 1958, **3**, 223–228.
29. J. I. Langford, D. Louër and P. Scardi, *J. Appl. Crystallogr.*, 2000, **33**, 964-974.
30. P. Scardi and M. Leoni, *Acta Crystallogr., Sect. A: Found. Adv.*, 2001, **57**, 604-613.
31. E. P. Wohlfarth and K. H. J. Buschow, *Ferromagnetic materials : a handbook on the properties of magnetically ordered substances*, North-Holland Pub. Co., Amsterdam; New York, 1980.
32. P. Ayyub, V. R. Palkar, S. Chattopadhyay and M. Multani, *Phys. Rev. B*, 1995, **51**, 6135–6138.
33. N. Lock, M. Christensen, K. M. Ø. Jensen and B. B. Iversen, *Angew. Chem. Int. Ed.*, 2011, **50**, 7045-7047.
34. K. M. Ø. Jensen, H. L. Andersen, C. Tyrsted, E. D. Bojesen, A.-C. Dippel, N. Lock, S. J. L. Billinge, B. B. Iversen and M. Christensen, *ACS Nano*, 2014, **8**, 10704-10714.
35. T. Egami and S. J. L. Billinge, *Underneath the Bragg Peaks*, Pergamon, Oxford, 2003.
36. C. Tyrsted, N. Lock, K. M. Ø. Jensen, M. Christensen, E. D. Bojesen, H. Emerich, G. Vaughan, S. J. L. Billinge and B. B. Iversen, *IUCrJ*, 2014, **1**, 165-171.
37. D. Saha, K. M. Ø. Jensen, C. Tyrsted, E. D. Bøjesen, A. H. Mamakhel, A.-C. Dippel, M. Christensen and B. B. Iversen, *Angew. Chem. Int. Ed.*, 2014, **53**, 3667-3670.
38. C. Weidenthaler, *Nanoscale*, 2011, **3**, 792-810.
39. N. Bao, L. Shen, W. An, P. Padhan, C. Heath Turner and A. Gupta, *Chem. Mater.*, 2009, **21**, 3458-3468.
40. C. N. Chinnasamy, B. Jeyadevan, K. Shinoda, K. Tohji, D. J. Djayaprawira, M. Takahashi, R. J. Joseyphus and A. Narayanasamy, *Appl. Phys. Lett.*, 2003, **83**, 2862-2864.
41. G. F. Goya, T. S. Berquo, F. C. Fonseca and M. P. Morales, *J. Appl. Phys.*, 2003, **94**, 3520-3528.
42. W. S. Seo, H. H. Jo, K. Lee, B. Kim, S. J. Oh and J. T. Park, *Angew. Chem. Int. Ed.*, 2004, **43**, 1115-1117.
43. S. A. Majetich, T. L. Wen and O. T. Mefford, *Mrs Bull.*, 2013, **38**, 899-903.

Nanoscale Accepted Manuscript